Journal of Sol-Gel Science and Technology (2019) 92:101–115
https://doi.org/10.1007/s10971-019-05080-6

ORIGINAL PAPER: NANO- AND MACROPOROUS MATERIALS (AEROGELS, XEROGELS, CRYOGELS, ETC.)

Check for updates

Influences of solvothermal-assisted crystallization process on the microstructure and properties of SiO_2-$W_{0.02}TiO_{2.06}$ composite aerogels synthesized via ambient pressure drying

Fei Shi[1] · Jia Liu[1] · Jingxiao Liu[1] · Xia Huang[1] · Shicheng Hu[1] · Dongyang Liu[1] · Yongqiang Wang[1] · Zhengjie Shan[1]

Received: 3 August 2018 / Accepted: 11 July 2019 / Published online: 29 July 2019

Abstract

In this work, the influence of solvothermal crystallization processes on the microstructure, pore characteristic, and adsorption/photocatalysis of SiO_2-$W_{0.02}TiO_{2.06}$ composite aerogels synthesized via ambient pressure drying have been investigated. It has been clarified that the composite aerogels prepared via solvothermal crystallization at 120 °C for 0.5 h and 180 °C for 3 h exhibited high-specific surface area (416–729 m^2/g) and pore volume (2.26–2.70 cm^3/g). With the increase of solvothermal crystallization temperature and time, the crystallinity of composite aerogels increased gradually, but excessive solvothermal crystallization time at higher temperature decreased the pore volume greatly. Furthermore, it is found that bacterial cellulose (BC) in the composite gel plays an important role in enhancing the pore volume and crystallization of the SiO_2-$W_{0.02}TiO_{2.06}$ composite aerogels as a pore-expanding agent and structure-directing agent. The as-synthesized SiO_2-$W_{0.02}TiO_{2.06}$ composite aerogels exhibited higher adsorption and removal efficiency for RhB than the commercial P25-TiO_2, which can be ascribed to its high pore volume and specific surface area, as well as the synergistic action of adsorption and photocatalysis.

Graphical Abstract

Influences of solvothermal crystallization on preparing SiO_2-$W_{0.02}TiO_{2.06}$ aerogels via ambient pressure drying have been investigated. Appropriate solvothermal crystallization process is favorable for achieving higher pore volume and crystallization of the composite aerogels. Bacterial cellulose (BC) in the composite gel plays an important role as a pore-expanding agent and structure-directing agent. The as-prepared SiO_2-$W_{0.02}TiO_{2.06}$ composite aerogels showed synergistic effect of adsorption and photocatalysis.

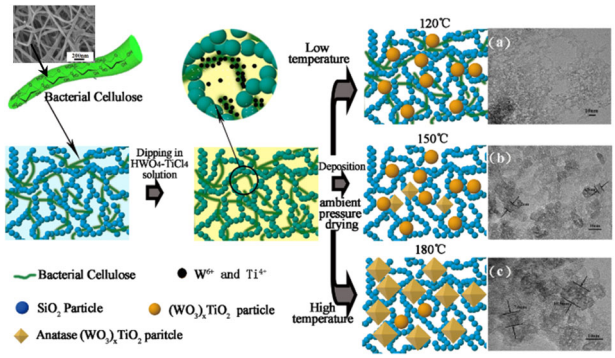

✉ Fei Shi
shifei@dlpu.edu.cn

✉ Jingxiao Liu
jxliu2366@163.com

[1] Key Laboratory of New Materials and Modification of Liaoning Province, School of Textile and Materials Engineering, Dalian Polytechnic University, 116034 Dalian, People's Republic of China

Highlights

- Effects of solvothermal crystallization on preparing SiO_2-$W_{0.02}TiO_{2.06}$ aerogels were investigated.
- Solvothermal process can greatly promote the crystallization of the composite aerogels.
- Appropriate solvothermal process is favorable infor achieving higher pore volume of aerogels.
- The SiO_2-$W_{0.02}TiO_{2.06}$ composite aerogels showed synergistic effect of adsorption and photocatalysis.

Keywords Composite aerogel · SiO_2 · $W_{0.02}TiO_{2.06}$ · Solvothermal crystallization · Adsorption · Photocatalysis

1 Introduction

At present, porous adsorbent materials such as silica aerogels, carbon aerogels, and graphene aerogels with excellent adsorption properties have been studied extensively. As it is reported, silica aerogels are efficient for adsorptive removal of naphthalene from aqueous solution [1]. Ultralight carbon aerogels synthesized from nano-cellulose exhibited highly selective oil adsorption [2], and carbon fiber aerogels made from raw cotton showed efficient and recyclable adsorption for oils and organic solvents [3]. In addition, flexible graphene aerogels [4], graphene/nano-fibrillated cellulose aerogel [5], and magnetic polystyrene/Fe_3O_4/graphene aerogel composites [6] were all shown to have superior adsorption properties.

Nevertheless, using porous photocatalysts with high adsorptivity and photocatalytic activity is a more effective way for removing dye pollutants in wastewater [7, 8]. To date, aerogel-based photocatalysts [9–12] and photocatalyst-loaded composite aerogels or porous materials [13–18] have been attracting considerable research interests as highly efficient environmental purification materials, because the integration of porous materials and photocatalyst may be conducive to performing the function of adsorption and photocatalysis simultaneously. Silica aerogels are unique porous materials with high optical transmittance and strong adsorptivity due to their large-specific surface area and pore volume [19–21]. Thus, it is of significance to develop a photocatalyst-SiO_2 composite aerogel with higher adsorptivity and visible light photocatalytic activity so as to remove efficiently the pollutants in the environment.

In order to achieve higher adsorption and photocatalytic efficiency of photocatalyst-SiO_2 composite aerogel, effective strategies should start from important factors such as the type of photocatalysts, the pore-forming mechanism and especially the fabrication process of composite aerogels. As is well known, TiO_2 is a photocatalyst exhibiting relatively high photocatalytic activity under irradiation of ultra-violet light. Over the past few years, many studies have been carried out by sensitizing TiO_2 with a narrower band-gap semiconductor such as CdS (2.4 eV), WO_3, or other metal and non-metals— such as Sb, Cr, C, etc—so as to further improve the visible-light-driven photocatalytic efficiency of TiO_2 [22–28]. In the meantime, mesoporous anatase TiO_2 was also reported for its efficient photocatalytic performance [29]. In addition, co-assembly of Au and TiO_2 particles into multicomponent 3D aerogels was also reported [30].

Apart from the process optimization for producing aerogels, another powerful strategy for enhancing porous structure and adsorption is utilizing templates such as bacterial cellulose (BC) in the synthesis of aerogel materials [31, 32]. Bacterial cellulose (BC) is an organic compound with the formula ($(C_6H_{10}O_5)_n$) produced from certain types of bacteria. It was reported that BC could be used for improving the porous structure of the aerogel, and flexible aerogels with interpenetrating network structure could be obtained by freeze drying of BC-silica composite gels [33]. It was also demonstrated that BC could be used as a suitable template for synthesizing $CoFe_2O_4$ by immersing it in the $FeSO_4/CoCl_2$ solution, and in this way a lightweight porous magnetic aerogel could be synthesized [34]. By comparison with other well-known structure-directing agents such as cetyltrimethylammonium bromide (CTAB) and sodium dodecyl sulfate (Lauryl SDS), the advantage of using bacterial cellulose as template is that porous materials with higher porosity and larger pore size could be easily obtained. For example, porous TiO_2-anatase films prepared using CTAB and SDS as templates exhibited pore sizes of only 1.5–3.1 nm [35]. In contrast, our recent research demonstrated that SiO_2-$(WO_3)_x$·TiO_2 composite aerogels prepared using bacterial cellulose as template showed higher pore sizes of 13 nm and pore volume with 1.33 cm^3/g compared to those obtained without BC template (with pore size and pore volume being 8 nm and 0.86 cm^3/g, respectively) [36].

In our previous research, we also investigated the effects of different templates such as ginkgo biloba leaf, starch, and BC on the specific surface area and pore volume of SiO_2-$W_{0.02}TiO_{2.06}$ composite aerogels prepared by a similar solvothermal method. The BET analysis results indicated that the composite aerogels with the highest specific surface area and pore volume were obtained by using BC as template rather than Ginkgo biloba leaf and starch, which demonstrated that BC has advantages over ginkgo biloba leaf and starch as templates.

In general, multicomponent aerogels can be prepared from wet gels by supercritical drying [30], or freeze drying [37]. However, the harsh preparation process with higher pressure/temperature or extreme lower temperature is not convenient for production on a large scale. Moreover, as for the photocatalyst-loaded silica aerogels, how to guarantee attaining highly porous structures and loading more photocatalyst particles with higher crystallinity into the composite aerogels simultaneously has been a challenge. In our previous research, synthesis of SiO_2-W_xTiO_2 composite aerogels via solvothermal crystallization followed by freeze drying was conducted [38], and a highly porous SiO_2-$(WO_3)_x$•TiO_2 composite aerogel was prepared by an ambient pressure drying method with a solvothermal-assisted crystallization process [36]. However, the effect of solvothermal crystallization process on the microstructure and properties of the composite aerogels needs to be further investigated.

Therefore, in this work, the influence of solvothermal crystallization on the microstructure, pore characteristics, and adsorption/photocatalytic activity of SiO_2-$W_{0.02}TiO_{2.06}$ composite aerogels synthesized via ambient pressure drying has been investigated systematically. The results are helpful for preparing SiO_2-$W_{0.02}TiO_{2.06}$ composite aerogels with higher adsorption and photocatalytic activity. Moreover, it is also significant for preparing other multicomponent oxide composite aerogels with functional properties.

2 Experimental

2.1 Synthesis of SiO_2-BC composite gel

The SiO_2-BC composite gel was synthesized by using industrial water glass ($Na_2O{\cdot}nSiO_2$ with $n = 3.5$, density = 1.53 g/cm^3) as silica source. First, the water glass was diluted with deionized water (the volume ratio of water glass/deionized water = 1:6), and then ion-exchanged with strongly acidic cation-exchange resin 732, to obtain silicic acid of pH = 2–3. The bacterial cellulose (BC, Shanghai Yifang Rural Technology Holdings Co. Ltd) was heated to 90 °C in a 2 M KOH solution for 6 h, and the darkened BC obtained was washed repeatedly with deionized water until it was translucent, so as to remove sugar. After that, the BC was made into a slurry with a juicer (the volume ratio of BC/deionized water = 1:1). Then, the BC/SiO_2 composite sol was obtained by mixing the BC slurry with the silicic acid (the volume ratio of silicic acid/slurry = 10:1). Finally, the pH of the composite sol was adjusted to 6–7 with 2 M ammonia solution, and after aging for 20 min the BC-SiO_2 composite gel was obtained.

2.2 Preparation of SiO_2-$W_{0.02}TiO_{2.06}$ composite aerogels

The BC-SiO_2 composite gel, after aging for 2 h at room temperature, was divided into small pieces with volumes of around 1 cm^3 and immersed in the WO_3-TiO_2 precursor solution for 24 h. The WO_3-TiO_2 precursor solution was prepared by mixing $TiCl_4$ and H_2WO_4 solution with a molar ratio of W/Ti = 2%. Then the gel was transferred to a 200 mL Teflon-lined autoclave with addition of 100 mL ethanol and underwent solvothermal reaction at 120–180 °C for 0.5–12 h. After that, surface modification of the SiO_2-$W_{0.02}TiO_{2.06}$ composite gel obtained was conducted in a mixed trimethylchlorosilane (TMCS)/hexane (V_{TMCS}: V_{hexane} = 1:10) solution for 1–3 days until the gel could be floated on water. Finally, the modified gel was dried successively at 80, 100, and 150 °C for 2 h, respectively, yielding light-weight porous SiO_2-$W_{0.02}TiO_{2.06}$ composite aerogels. For comparison, SiO_2-$W_{0.02}TiO_{2.06}$ composite aerogels without using BC and solvothermal crystallization were also prepared according to the aforementioned method. According to our previous research, the as-prepared composite aerogels by the above method are hydrophobic [39]. In this work, hydrophilic composite aerogels were obtained after heat-treated at 500 °C for 2 h.

2.3 Characterization

X-ray diffraction (XRD) analysis was carried out by X-ray diffraction (D/Max-3B, Japan) using Cu anode target, tube voltage of 40 kV and tube current of 45 mA. The micromorphology of the composite aerogels was observed using a field emission scanning electron microscope (FESEM, Hitachi S-4800, Japan) with accelerating voltage 5.0 kV and transmission electron microscope (TEM, JEOL JEM-2100 UHR) with accelerating voltage 200 kV. The specific surface area and pore characteristics of SiO_2-$W_{0.02}TiO_{2.06}$ composite aerogels were measured using a N_2 adsorption-desorption specific surface area analyzer (SSA-4200, Beijing Biaode Electronic Technology Co. LTD). The specific surface area was calculated from N_2 physisorption data using the Brunauer-Emmet-Teller (BET) equation. Pore volume and pore size distributions were obtained by the Barrett-Joyner-Halenda (BJH) method from the desorption stage. Differential thermal analysis (DTA, WCR-2D, Beijing Optical Instrument Factory) was used to analyze the thermal evolution process of the composite aerogels obtained.

2.4 Adsorption and photocatalytic activity tests

Rhodamine B (RhB), also known as rose red B, is mainly used for industrial dyeing. Once RhB enters the human

body, it can form carcinogens through biological transformation. Hence, removing RhB from industrial wastewater is necessary for human health. In this experiment, RhB was used for evaluating the adsorption/photocatalytic activity of the SiO_2-$W_{0.02}TiO_{2.06}$ composite aerogels. First, 0.1 g of SiO_2-$W_{0.02}TiO_{2.06}$ composite aerogel, heat-treated at 500 °C for 2 h, was added into a 250 mL beaker together with 100 mL of a 1×10^{-5} M RhB solution. Following our previous work, adsorption experiments were first conducted in a darkroom for 60 min. During the adsorption experiment, the RhB solution was stirred in the dark environment. At regular intervals, take the upper clear supernatant liquid and have a centrifugal separation process. Then the optical absorbance of the upper clear supernatant liquid was measured using a UV–Vis spectrophotometer (UV751 GD) at a wavelength of 554 nm. After the adsorption experiment, the visible light photocatalytic experiment was performed by irradiating the sample for different times with a light intensity of 5.0 mW/cm^2 using a high-pressure mercury lamp (125 W, $\lambda > 380$ nm) as light source. Finally, the concentration of RhB solution after adsorption/photocatalysis for different time can be determined according to the standard curve relating the absorbance and concentration of RhB standard solutions, and the adsorption/photocatalytic degradation rate can be calculated according to the following equation:

$$\eta = \left(1 - \frac{C}{C_0}\right) \times 100\%,$$

in which η is the adsorption rate or photocatalytic degradation rate, C_0 is the initial concentration of the RhB solution before adsorption or photocatalysis, and C is the concentration after adsorption or photocatalytic degradation for a period of time.

In order to evaluate the recycling performance of the as-prepared SiO_2-$W_{0.02}TiO_{2.06}$ composite aerogels, the composite aerogels with solvothermal crystallization at 180 °C for 3 h and after heat-treatment at 500 °C for 2 h were selected to investigate the recyclable adsorption/photocatalytic degradation performance under simulated solar light. The adsorption and photocatalytic degradation of RhB were conducted at the same time. During the adsorption/photocatalysis experiment, the RhB solution containing SiO_2-$W_{0.02}TiO_{2.06}$ composite aerogel samples were irradiated for different times using a metal halide lamp (ZY73-TD, 150 W) with the distance between the lamp and sample being about 64 cm. After each cycle, the sample was washed with water and ethanol for three times and was then dried under the metal halide lamp (ZY73-TD, 150 W) so as to remove surface adsorbates and restore the adsorption/photocatalytic activity.

3 Results and discussion

Figure 1a shows the XRD patterns of the SiO_2-$W_{0.02}TiO_{2.06}$ composite aerogels synthesized at different solvothermal crystallization temperatures. It can be seen that with the increase of solvothermal crystallization temperature, the crystallinity of composite aerogels increased gradually. Figure 1b shows the XRD patterns of the composite aerogels prepared via solvothermal crystallization at 180 °C for different time. It is obvious that anatase crystals appeared in all of the composite aerogels prepared via solvothermal crystallization at 180 °C for different time. In addition, the crystallinity of the composite aerogels increased significantly with the extension of solvothermal crystallization time.

The FWHM (full-width at half-maximum) of the XRD diffraction peak corresponding to the anatase (101) crystal plane decreases with an increase of solvothermal

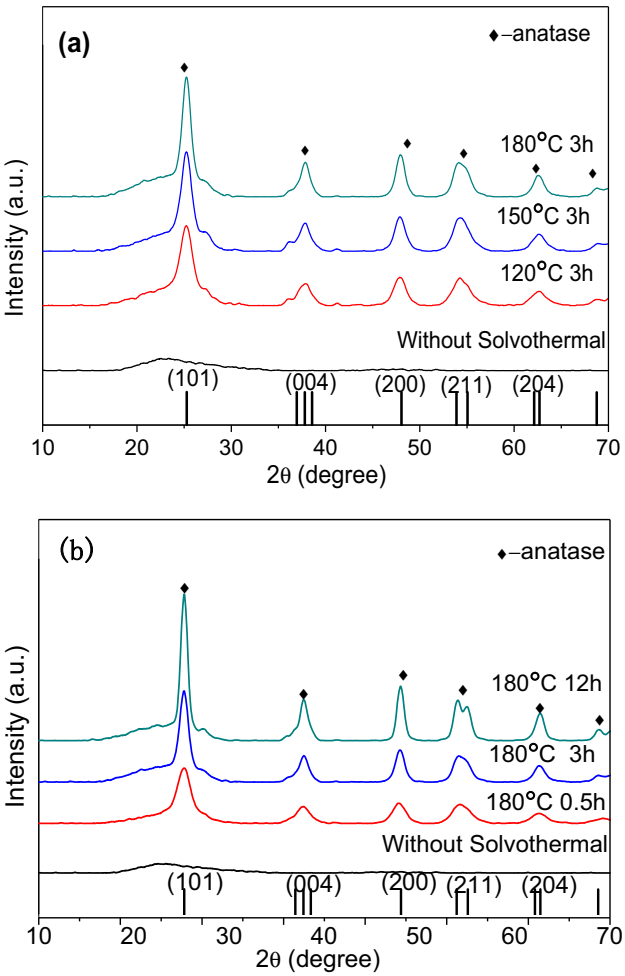

Fig. 1 XRD patterns of the composite aerogels using different solvothermal crystallization process parameters: **a** solvothermal crystallization for 3 h at different temperature; **b** solvothermal crystallization at 180 °C for different time

crystallization time, which is related to the grain growth of the $W_{0.02}TiO_{2.06}$ nanoparticles distributed in the network structure of the aerogels. Moreover, the crystallite size of the SiO_2-$W_{0.02}TiO_{2.06}$ composite aerogels has been calculated using the Scherrer equation, as shown in Table 1. The Scherrer equation is as follows:

$$\tau = \frac{k\lambda}{\beta \cos\theta}$$

Table 1 The crystallite size of the SiO_2-$W_{0.02}TiO_{2.06}$ composite aerogels prepared with different solvothermal crystallization temperature and time

The precursor gel	Solvothermal temperature (°C)	Solvothermal time (h)	Crystal size (nm)
BC-SiO_2	120	3	4.8
BC-SiO_2	150	3	5.9
BC-SiO_2	180	0.5	4.8
BC-SiO_2	180	3	7.2
BC-SiO_2	180	12	9.5

where t is the crystallite size; k is the shape factor with a typical value of about 0.9; λ is the X-ray wavelength; β is the line broadening at half the maximum intensity (FWHM); and θ is the Bragg angle (in degrees).

The SEM images of the SiO_2-$W_{0.02}TiO_{2.06}$ composite aerogels are shown in Fig. 2. It can be observed that the composite aerogels show a porous morphology, which indicates that the porous aerogel network could still be obtained by surface modification and ambient pressure drying after the solvothermal crystallization process. Moreover, the composite aerogels prepared using different solvothermal crystallization conditions exhibit different porous morphologies, indicating that the solvothermal crystallization process has a significant effect on the pore characteristics of the composite aerogels (see Fig. 2a–c). In addition, the composite aerogel obtained with solvothermal crystallization in the presence of BC exhibits a more high porous structure than that without BC (Fig. 2d).

The TEM images of the as-prepared composite aerogels with different solvothermal crystallization process parameters are shown in Fig. 3. It can be seen that the nanocrystalline grains are embedded in the porous network. With the increase in solvothermal temperature and time, the size

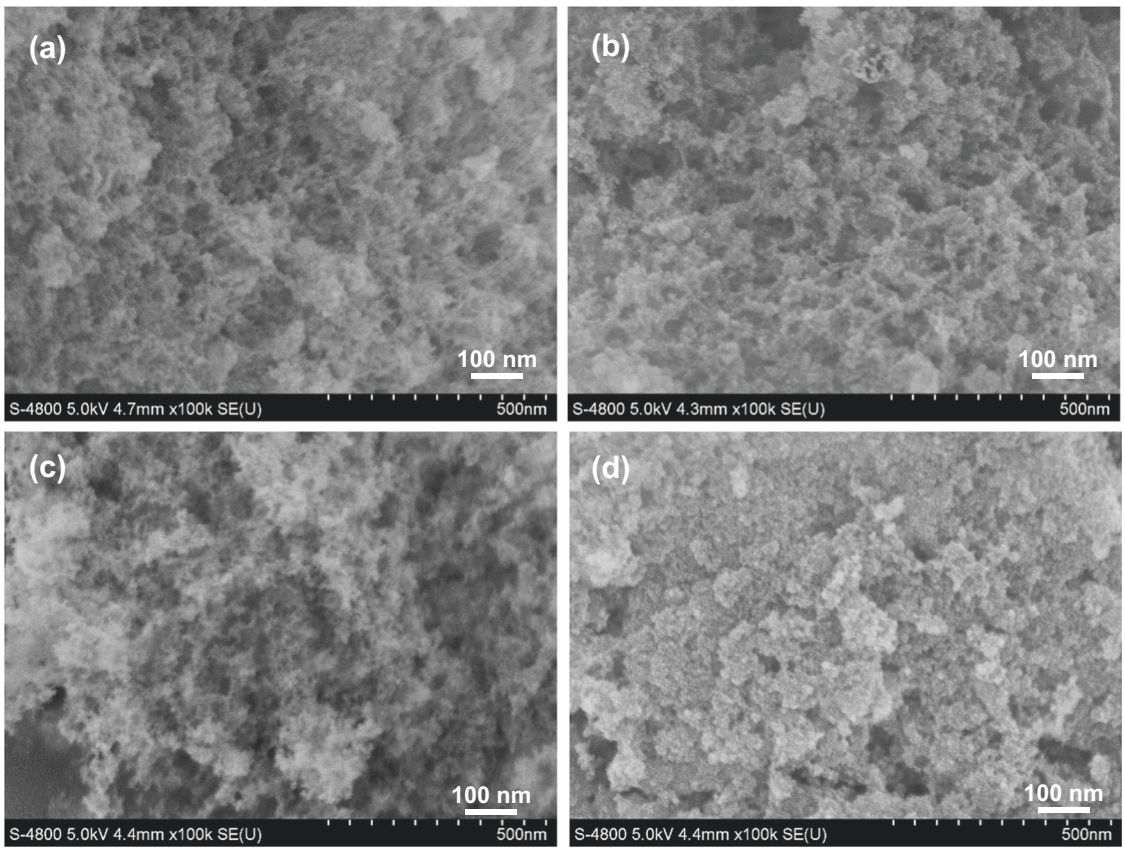

Fig. 2 SEM images of the aerogels synthesized with different solvothermal crystallization conditions: **a** 120 °C, 1 h; **b** 120 °C, 3 h; **c** 180 °C, 12 h; **d** 150 °C, 3 h without BC

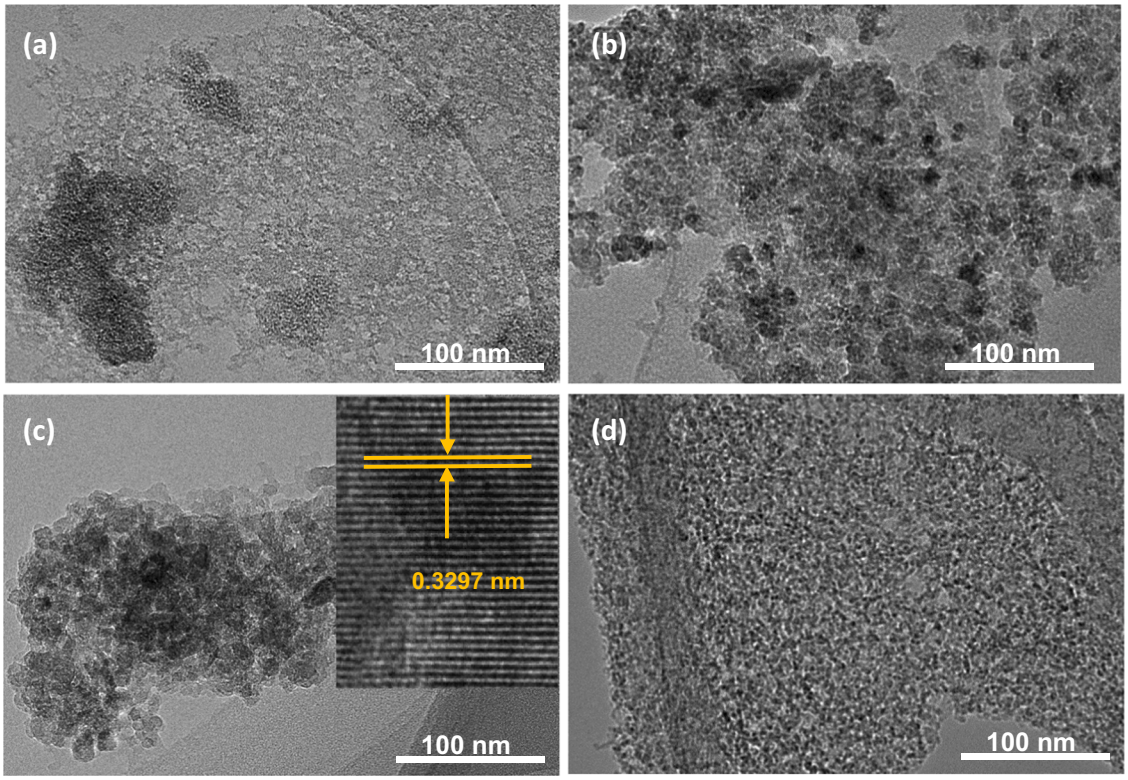

Fig. 3 TEM images of the composite aerogels prepared with different solvothermal crystallization process parameters: **a** 120 °C, 3 h; **b** 180 °C, 3 h; **c** 180 °C, 12 h; **d** BC-SiO_2 aerogel (The pure SiO_2 aerogel without loaded $(WO_3)_x{\cdot}TiO_2$ particles was prepared by a similar method via ambient-pressure drying with solvothermal crystallization at 180 °C for 3 h)

of the $W_{0.02}TiO_{2.06}$ crystallites gradually increases. In particular, $W_{0.02}TiO_{2.06}$ grains with well-defined crystallinity can be seen clearly in the composite aerogels with solvothermal crystallization at 180 °C for 12 h (Fig. 3c). In contrast, the pure SiO_2 aerogel samples synthesized without immersing the gel into $TiCl_4/H_2WO_4$ solution only shows the porous network characteristic without any crystal grains evident in the TEM image (Fig. 3d).

The results of the N_2 adsorption analysis of the composite aerogels are shown in Fig. 4. The N_2 adsorption-desorption isotherms in Fig. 4a, b exhibit type IV curves with hysteresis loop between type H_2 and H_3 according to the IUPAC classification. This result indicates that the composite aerogels obtained have the typical characteristics of mesoporous materials, and the pore shape will vary with the solvothermal crystallization time. Figure 4c, d shows the pore size distributions of the composite aerogels. The pore diameter of the composite aerogels obtained with solvothermal crystallization at 120 °C is in the range of 4–12 nm. The pore size increases with increasing solvothermal time from 2 to 3 h, which can be ascribed to the hydrolysis of BC. The pore diameter of the composite aerogels prepared by solvothermal crystallization at 180 °C is in the range of 5–13 nm. These changes in the pore diameter of the SiO_2-$W_{0.02}TiO_{2.06}$ composite aerogels can be explained as follows. On one hand, the BC will hydrolyze during the solvothermal crystallization process, which would be expected to result in an increase in the pore diameter. On the other hand, $W_{0.02}TiO_{2.06}$ particles will deposit in the pores and on the surface of the SiO_2 particle at the same time, which will reduce the pore size to some extent, due to the growth of $W_{0.02}TiO_{2.06}$ particles.

A proposed mechanism for the formation of SiO_2-$W_{0.02}TiO_{2.06}$ composite aerogels prepared with solvothermal crystallization in the presence of BC is illustrated in Fig. 5. During the solvothermal crystallization, the hydrolysis of BC and deposition of $W_{0.02}TiO_{2.06}$ nanoparticles will occur simultaneously, which play an important role in controlling the final pore size and pore volume of the composite aerogels. Under condition involving sufficient solvothermal crystallization and complete hydrolysis of BC, the composite gel network will only be composed of SiO_2 gel and $W_{0.02}TiO_{2.06}$ nanoparticles.

It would be expected that the strongly polar hydroxyl groups produced by the hydrolysis of BC will promote the deposition of $W_{0.02}TiO_{2.06}$ particles on the surface of the pores in the composite gels. At lower temperatures, $W_{0.02}TiO_{2.06}$ nanoparticles will first grow on the surface of BC during the solvothermal crystallization process. Subsequently, the BC will hydrolyze into glucose with increasing

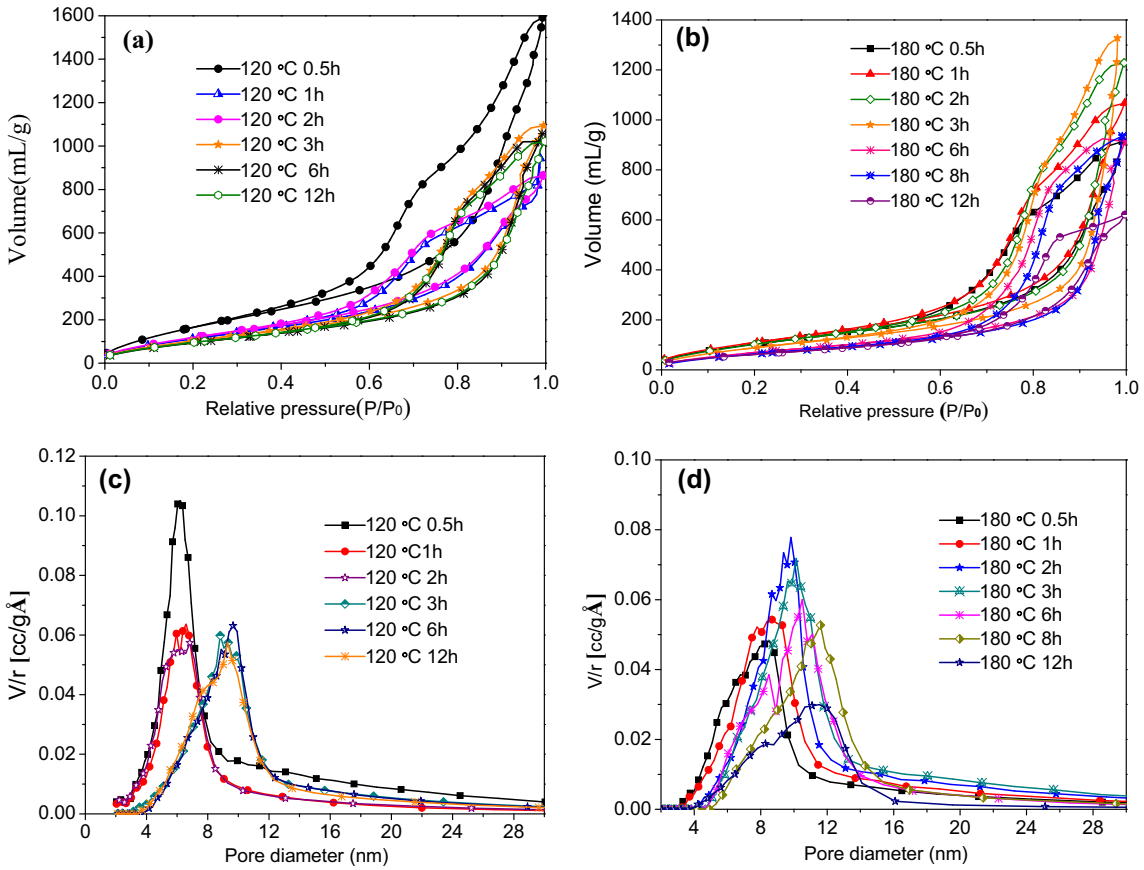

Fig. 4 N_2 adsorption-desorption isotherms **a** and **b** and pore size distributions **c** and **d** of the composite aerogels synthesized using different solvothermal crystallization conditions before surface modification and ambient pressure drying

solvothermal crystallization temperature and time [36]. Then, the generated glucose will play a role as the inducer and cross-linking agent to further induce the deposition of $W_{0.02}TiO_{2.06}$ particles and link the $W_{0.02}TiO_{2.06}$ grains with the SiO_2 gel.

As is shown in Fig. 5, when the gel is dipped in the H_2WO_4-$TiCl_4$ solution, W^{6+} and Ti^{4+} ions will sorb on the surface of BC. Then, during the solvothermal crystallization, the hydrolysis of BC and deposition of $W_{0.02}TiO_{2.06}$ particles into the network of composite gels will occur simultaneously. As a result, the composite aerogels with different surface morphologies can be obtained under different solvothermal crystallization conditions. When the solvothermal crystallization temperature and time is 120 °C and 3 h, respectively, only a small amount of $W_{0.02}TiO_{2.06}$ particles deposited onto the surface of BC and pore walls, and the as-prepared composite aerogel exhibits a highly porous network structure. When the solvothermal crystallization temperature and time are increased to 150 °C and 3 h, respectively, the amount of $W_{0.02}TiO_{2.06}$ particles deposited onto the pore walls will increase, as can be observed clearly in the TEM images. As is shown in Fig. 5b, the lattice fringes (0.35 nm) corresponding to the (101) [40] reflection plane of anatase can be observed, with the scope of lattice fringes ranging from 4.5 nm to 7.2 nm. When the solvothermal crystallization temperature rises to 180 °C (Fig. 5c), the scope of lattice fringes increases from 7.6 nm to 10.9 nm, which indicates that the anatase grains can grow significantly under the latter conditions.

Therefore, it is evident that the pore volume of the composite aerogels and the amount of $W_{0.02}TiO_{2.06}$ nanoparticles deposited onto the pore wall can be controlled by adjusting the solvothermal condition. During the solvothermal crystallization process, BC plays an important role in the formation of the porous structure and deposition of $W_{0.02}TiO_{2.06}$ particles. On one hand, BC plays a role as pore-expanding agent, and the decomposition of BC will be conducive to increasing the pore volume of the composite aerogels. On the other hand, BC functions as a structure-directing agent, and the decomposition of BC will induce the deposition and growth of $W_{0.02}TiO_{2.06}$ nanoparticles. Thus, solvothermal crystallization in the presence of BC is very favorable for obtaining SiO_2-$W_{0.02}TiO_{2.06}$ composite aerogels with higher pore volume and $W_{0.02}TiO_{2.06}$ crystallites, simultaneously. Furthermore, this method is also

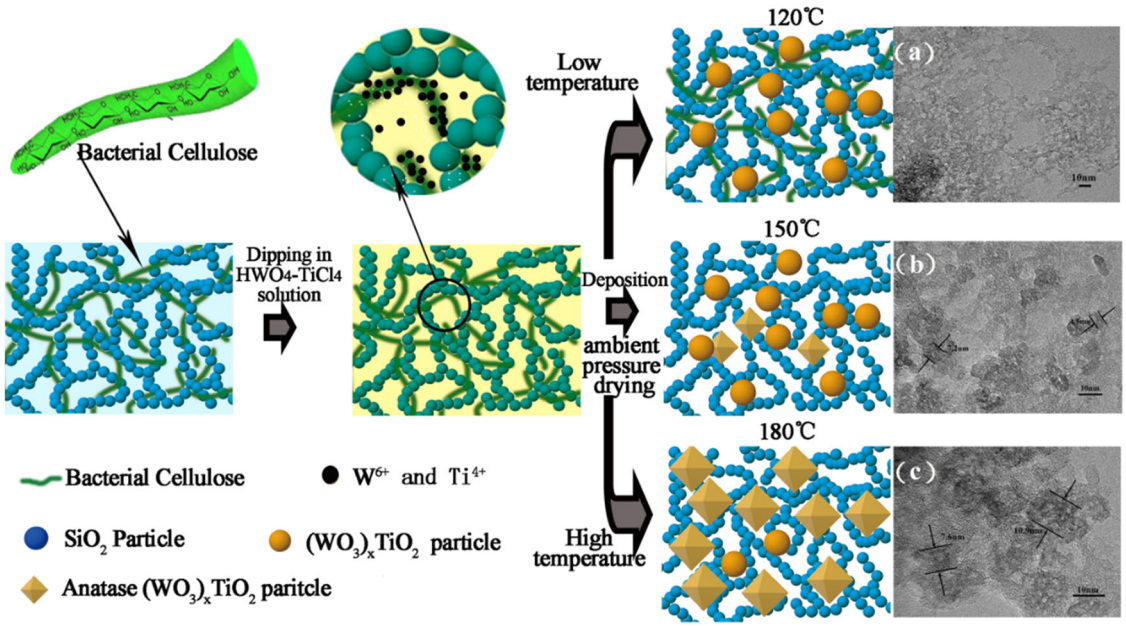

Fig. 5 Proposed mechanism for the formation of SiO_2-$W_{0.02}TiO_{2.06}$ aerogels with solvothermal crystallization in the presence of BC and the corresponding TEM images of the as-prepared composite aerogels: **a** 120 °C, 3 h; **b** 150 °C, 3 h; **c** 180 °C, 3 h

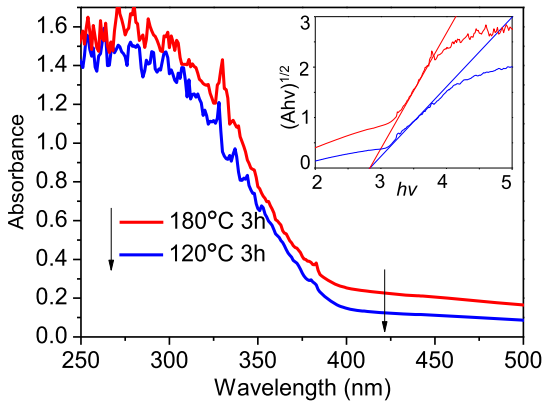

Fig. 6 UV-Vis absorption spectra of the composite aerogels with solvothermal crystallization at different temperature for 3 h

suitable for preparing other multicomponent composite aerogel materials.

The UV-Vis absorption spectra and $(Ahv)^{1/2}$-hv relationship of the composite aerogels are shown in Fig. 6. The composite aerogels synthesized with solvothermal crystallization at 120 °C have lower absorption of UV light, which is presumably due to the lower amount of $W_{0.02}TiO_{2.06}$ particles deposited onto the pore wall in the composite aerogels. In addition, the high visible light absorption of the composite aerogels with solvothermal crystallization at 180 °C indicates that it may have improved visible-light-driven photocatalytic activity compared to the 120 °C-solvothermal sample.

It is also reasonable that the optical absorption of the composite aerogels in the visible light region would be enhanced with the increase of crystallinity and grain growth. The calculated band gap of the composite aerogels is in the range of 2.75–2.8 eV, obviously lower than that of pure TiO_2 (3.2 eV).

Figure 7 shows the effects of heat treatment on the network structure and surface hydrophobicity/hydrophilicity of the composite aerogels. The DTA curves of BC and the composite aerogels obtained with solvothermal crystallization at 180 °C for 12 h are shown in Fig. 7a. It can be seen that the BC has a stronger exothermic peak at 300 °C corresponding to its combustion. In comparison, the as-prepared composite aerogel has a smaller exothermic peak at 253 °C, which is due to the combustion of the intermediate product produced by BC hydrolysis during the solvothermal process. Figure 7b shows the photographs of the composite aerogels floating on water. The contact angle with water of the composite aerogels prepared by solvothermal crystallization at 180 °C for 12 h before heat-treatment was measured to be 148°, indicating that the composite aerogels are highly hydrophobic. The hydrophobicity of the composite aerogels is related to the surface modification of the wet gel with TMCL. In contrast, the composite aerogels after heat-treatment can be entirely wetted by water. This result indicates that the transition between hydrophilicity and hydrophobicity of the composite aerogels can be realized by heat-treatment at 500 °C for 2 h.

As is shown in Fig. 7c, the super hydrophobicity caused by the methyl ($–CH_3$) groups associated with the absorption peak at 1380 cm^{-1} will disappear after heat treatment [41, 42]. After heat treatment, owing to the decomposition of $–CH_3$ groups, not only the composite aerogels with solvothermal crystallization at 180 °C for 12 h but also the aerogels with solvothermal crystallization at 120 °C for 12 h lose the peak at 1380 cm^{-1}. In addition, the absorption peak at 2965 cm^{-1} corresponding to stretching vibration of $–CH_3$ groups also disappeared or became weaker due to decomposition of the $–CH_3$ groups [43].

Variations in the specific surface area and pore volume of the composite aerogels with different solvothermal crystallization time, before and after heat-treatment at 500 °C are shown in Fig. 8. It is found that the solvothermal crystallization and heat-treatment process have a significant impact on the specific surface area and pore volume of the composite aerogels. During the solvothermal crystallization, the hydrolysis of BC will occur with formation of short chains of glucose. In the case of the composite aerogels with solvothermal crystallization at 120 °C, the composite aerogels obtained with solvothermal crystallization for 0.5 h have the largest specific surface area and pore volume. With the increase of solvothermal temperature and time, the extent of hydrolysis of BC will increase, which will lead to a decrease in specific surface area and pore volume. The composite aerogels with solvothermal crystallization at 120 °C for 0.5 h had the lowest hydrolysis extent of BC, thus highly porous composite aerogels with higher pore volume and specific surface area could be obtained owing to the function of BC as a pore-expanding agent. After heat-treatment, the composite aerogels with solvothermal crystallization at 120 °C have an obvious decrease in the pore volume, with the exception of the composite aerogel with solvothermal crystallization at 120 °C for 3 h. During heat-treatment, the thermal decomposition of intermediate products of BC such as polysaccharide and glucose will occur, and the resulting H_2O and Si–OH groups will lead to the formation of Van der Waals bonds and capillary forces between the SiO_2 particles, which will cause polymerization of the gel and decrease the pore volume.

In the case of the composite aerogels with solvothermal crystallization at 180 °C, the composite aerogels obtained with solvothermal crystallization for 3 h have the largest specific surface area and pore volume. This is attributed to a strengthening of the composite gel network during sol-

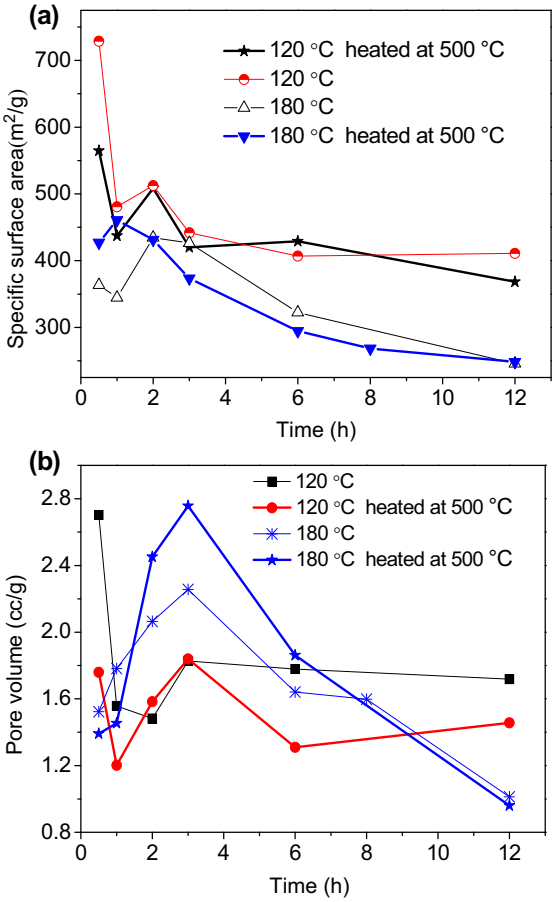

Fig. 8 Variations in the specific surface area **a** and pore volume **b** of the composite aerogels with different solvothermal crystallization temperature before and after heat-treatment

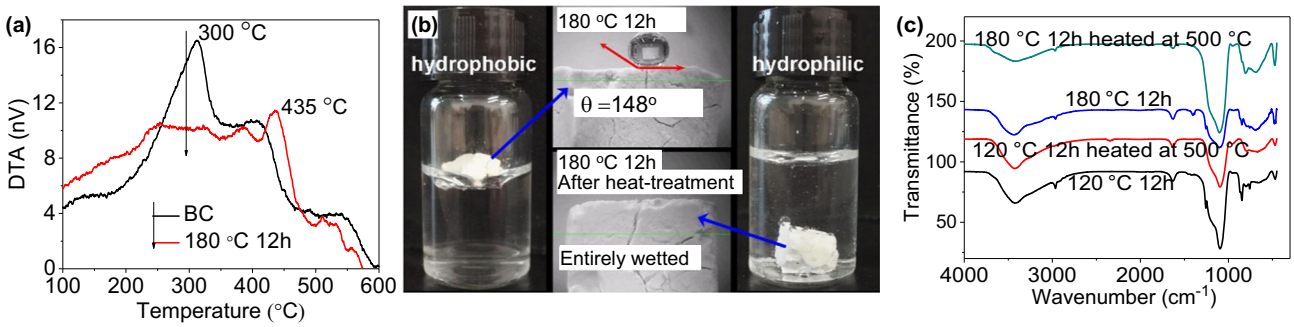

Fig. 7 **a** DTA curves of BC and composite aerogel prepared by solvothermal crystallization at 180 °C for 12 h; **b** photographs of hydrophobicity/hydrophilicity and contact angle with water of the composite aerogels; **c** FTIR spectra of the composite aerogels before and after heat-treatment

vothermal crystallization at 180 °C for 3 h, leading to highly porous composite aerogels after surface modification and ambient pressure drying. With the increase of solvothermal crystallization time at 180 °C, the amount of $W_{0.02}TiO_{2.06}$ particles deposited increased, which will lead to the decrease of pore volume. In addition, with the increase of solvothermal time at 180 °C, the composite gel network may become more compact, which will not be favorable for the following surface modification, and thus the pore volume would be expected to decrease. After heat-treatment, the composite aerogels with solvothermal crystallization at 180 °C for 2–6 h have an obvious increase in the pore volume. This is attributed to combustion of the residual organic groups after surface modification. Moreover, in this work, preparation of SiO_2-$W_{0.02}TiO_{2.06}$ composite aerogels without solvothermal crystallization was also conducted. However, it was found that the composite wet gels shrink significantly after surface modification without the solvothermal crystallization process and it was impossible to obtain a porous aerogel. This result is presumably due to the interactive polymerization between the undecomposed BC molecules, which would be expected to promote densification of the network with associated loss of porosity.

Figure 9 shows the adsorption/photocatalytic degradation and the corresponding adsorption kinetic rate curves of the composite aerogels prepared under different solvothermal conditions. As is shown in Fig. 9a, b, when the solvothermal crystallization time is less than 2 h, the adsorption of the composite aerogels plays an important role in removing the RhB from water due to its higher specific surface area and pore volume. It was found that the composite aerogels prepared using solvothermal time less than 2 h achieved adsorption equilibrium and surface saturation within 60 min, which is similar to the results previously reported for the adsorption of RhB on SiO_2 microsphere/graphene oxide composites [44]. As for the other composite aerogels with solvothermal processing times for more than 2 h, the adsorption saturation seems to occur more slowly, which may be ascribed to the slower diffusion of RhB molecules owing to the decreased pore volume and pore diameter. It would be expected that the composite aerogels processed with shorter solvothermal crystallization times would have a lower amount of $W_{0.02}TiO_{2.06}$ nanoparticles deposited in the network structure, and with the increase of solvothermal crystallization time, the maximum adsorption efficiency would hence decrease owing to the decreased pore volume.

Furthermore, owing to the lower band gap of the composite aerogels compared to P25, the formation of e^-/h^+ pairs can be excited by irradiation in the visible region. Thus, the composite aerogels should have better photocatalytic activity under the irradiation of visible light than P25. Although the photocatalytic activity in Fig. 9a, b does not appear to be as prominent as the adsorption, this may be ascribed to the lower amount of the residual RhB in the solution after adsorption.

It is found that the sample P25 also shows some photocatalytic activity under visible light irradiation, which may be ascribed to the RhB dye sensitization [45]. This result indicates that RhB dye sensitization may exist in the photocatalytic activity of the composite aerogels. In fact, relative comparison of pure redox forces in another visible light photocatalytic materials requires considering the effect of dye sensitization. As is shown in Fig. 9a, b, the composite aerogels can adsorb more RhB owing to its high pore volume and specific surface area than P25. Thus, the high adsorption efficiency of RhB in the composite aerogels are favorable for improving the dye sensitization, which is conducive to further improving the photocatalytic degradation efficiency of RhB. Hence, the synergistic effect of adsorption/photocatalytic degradation of RhB in the composite aerogels are more prominent. Therefore, the higher adsorption capacity and dye sensitization can achieve higher synergistic effect and jointly improve the efficiency of the composite aerogels for removing harmful RhB dye. In our next research, we will pay more attention to the dye sensitization and its effect on the photocatalytic activity of the composite aerogels.

Figure 9c, d show the adsorption kinetic rate curves for the composite aerogels. The adsorption has been carried out in the darkroom environment for 60 min. The adsorption performance for RhB of the composite aerogels decreases with increasing solvothermal crystallization time, whether the crystallization temperature is 120 or 180 °C. As is well known, the adsorption performance is related to the pore volume and specific surface area of the composite aerogels. With the increase of solvothermal crystallization time, the deposited $W_{0.02}TiO_{2.06}$ amount increases gradually, which will decrease the pore volume of the composite aerogels to some extent. However, all composite aerogels exhibit higher adsorptivity owing to their higher pore volumes and specific surface areas, which can promote relatively fast and efficient removal of pollutants in the environment.

The effects of BC and solvothermal conditions on the pore characteristics and adsorption/photocatalytic efficiency of SiO_2-$W_{0.02}TiO_{2.06}$ composite aerogels are shown in Table 2. It can be seen that SiO_2-$W_{0.02}TiO_{2.06}$ composite aerogels with pore volume V_{pore}å 0.5 cm^3/g cannot be obtained without solvothermal treatment from BC-SiO_2 composite gels, and accordingly exhibit little adsorption/photocatalytic activity. In contrast, the composite aerogels synthesized with solvothermal crystallization from pure SiO_2 gels, despite the lack of BC, have higher adsorption/photocatalytic efficiency than that obtained without solvothermal crystallization, which indicates that the solvothermal crystallization plays an important role in enhancing the adsorption and photocatalytic activity. Moreover, the

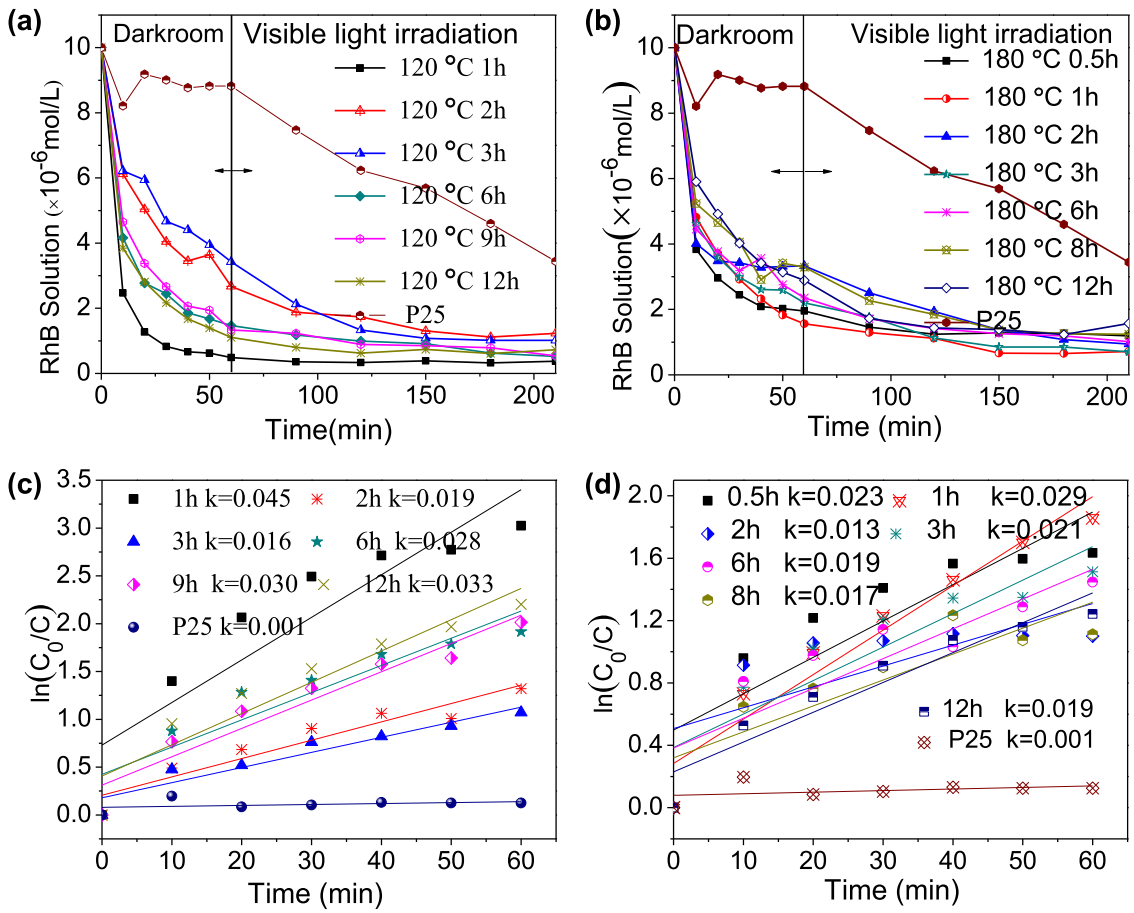

Fig. 9 **a** and **b** The adsorption/photocatalytic degradation curves; and **c** and **d** the corresponding adsorption kinetic rate curves of the composite aerogels with solvothermal crystallization at different temperature for different time

Table 2 The effects of BC and solvothermal condition on the properties of SiO_2-$W_{0.02}TiO_{2.06}$ composite aerogels

Precursor gel	Solvothermal temperature/time (°C/h)	BET SSA[a] (m^2/g)	Pore volume (cm^3/g)	Adsorption rate (η_1, %)	Photocatalytic efficiency (η_2, %)	Total APE[b] ($\eta_1+\eta_2$, %)
BC-SiO_2	No	222	0.20	0	0	0
SiO_2	No	312	0.69	58.9	0.3	59.2
SiO_2	150/0.5	267	1.05	82.2	0.8	83.6
BC-SiO_2	150/0.5	364	0.78	85.9	8.8	94.7
BC-SiO_2	120/1.0	480	1.46	**95.1**	1.1	**96.2**
BC-SiO_2	180/1.0	461	1.65	84.4	8.5	92.9
P25-TiO_2	–	61	0.77	11.8	53.8	65.6

[a]*SSA* specific surface area

[b]*APE* total adsorption/photocatalytic efficiency

The bold values mean that the sample has higher adsorption rate and total adsorption/photocatalytic efficiency than other samples. The purpose of bold is to highlight its excellent adsorption and photocatalytic efficiency

composite aerogel samples synthesized from BC-SiO_2 composite gels with solvothermal crystallization have apparently improved adsorption/photocatalytic efficiency. In particular, under appropriate solvothermal temperature and time, SiO_2-$W_{0.02}TiO_{2.06}$ composite aerogels with high adsorption/photocatalytic efficiency can be obtained.

In order to highlight the higher efficiency of the composite aerogels for RhB decomposition, the characteristics of the

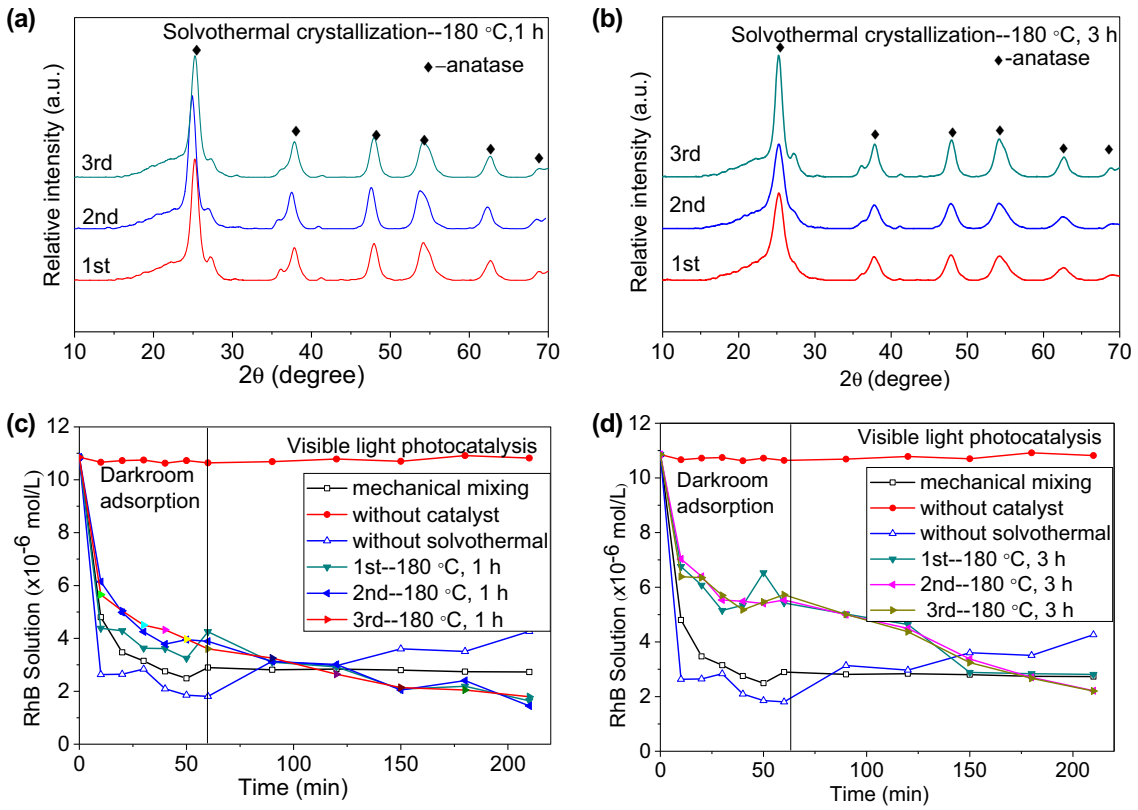

Fig. 10 The XRD (**a–b**) and adsorption/photocatalysis (**c–d**) of the composite aerogels prepared repeatedly under the same experimental conditions

P25-TiO_2 powders were also listed in Table 2. It is found that the P25-TiO_2 exhibits much lower specific surface area and adsorption rate than the composite aerogels. The adsorption rate within 60 min and the total adsorption/photocatalytic efficiency of the P25-TiO_2 sample for Rhodamine B after 210 min was only 11.8% and 65.6%, respectively. In contrast, the as-prepared composite aerogels from BC-SiO_2 gel exhibited higher total adsorption/photocatalytic efficiency with 92.9–96.2%. In particular, the adsorption rate of the composite aerogels is much higher than that of the P25-TiO_2 sample. Despite the higher photocatalytic activity of P25-TiO_2, the total adsorption/photocatalytic efficiency of composite aerogels is higher than that of the P25-TiO_2 sample. It is evident that the higher adsorption rate and removing efficiency of RhB of the composite aerogels is attributed to its higher pore volume and specific surface area. Moreover, the synergistic action of adsorption and photocatalysis of the composite aerogels may also help to achieve higher removing efficiency of RhB pollutants. The higher removing efficiency of RhB indicates that the as-prepared composited aerogels in this work have broad application prospects in the field of environmental purification.

Figure 10a, b shows the XRD patterns of the three samples of composite aerogels prepared via solvothermal crystallization at 180 °C for either 1 or 3 h (i.e., three samples at each time point). It is evident that the reproducibility of the sample preparation is excellent, with the slight differences in the intensity of the respective diffraction patterns being ascribed to minor inhomogeneity within the samples. Similarly, BET analysis results indicate that a deviation of less than ±0.15 cm^3/g of pore volume occurs in the repeat samples.

Figure 10c, d shows the adsorption/photocatalytic degradation curves of the two sets of triplicate samples. It can be observed that the respective triplicate samples all exhibit comparable high efficiency for removing RhB. The adsorption rate within 60 min and the total adsorption/photocatalytic efficiency for Rhodamine B after 210 min of the composite aerogel with solvothermal crystallization at 180 °C for 1 h is about 64 ± 3% and 85 ± 2%, respectively. This result indicates that the preparation process in this work is essentially reproducible.

In addition, in order to clarify the synergistic action of adsorption and photocatalysis of the composite aerogels, the adsorption/photocatalysis curves for a sample prepared without solvothermal crystallization and a sample prepared by mechanical mixing of SiO_2 aerogel with $W_{0.02}TiO_{2.06}$ particles are also illustrated in Fig. 10. It can be observed that the sample prepared by mechanical mixing exhibited almost no photocatalytic activity after the initial adsorption process,

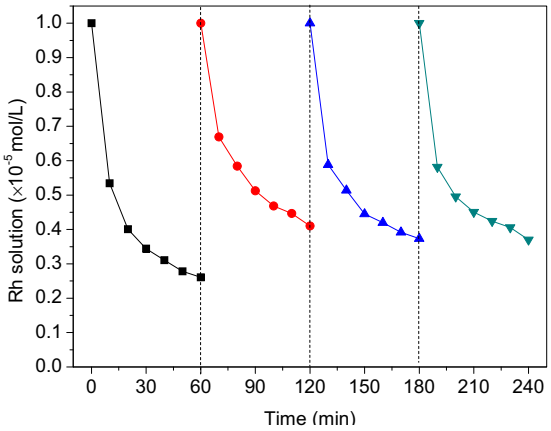

Fig. 11 The recycle results for the composite aerogels after heat-treatment at 500 °C for 2 h with initial solvothermal crystallization at 180 °C for 3 h (the specific surface area and pore volume were measured to be 416 m^2/g and 2.76 cm^3/g, respectively)

while the composite aerogel sample obtained without solvothermal crystallization even exhibits some desorption after the initial adsorption in the dark. This result indicates that the as-prepared composite aerogels in this work showed higher synergistic action of adsorption and photocatalytic activity, even though the SEM and TEM images show a random TiO_2 and WO_3 distribution in the SiO_2 network.

Furthermore, the photolysis curve of a catalyst-free RhB solution under irradiation is also illustrated in Fig. 10. It can be observed that almost no photolysis occurred under such conditions. This result further demonstrates that the as-prepared composite aerogels have good adsorption/photocatalytic properties.

Figure 11 shows the recycling results of the adsorption/photocatalysis of the composite aerogels after heat-treatment at 500 °C with solvothermal crystallization at 180 °C for 3 h. During the recycling tests, the adsorption/photocatalytic degradation for RhB was carried out simultaneously under irradiation using a metal halide lamp for 60 min. As is shown in Fig. 11, all the recycled composite aerogels exhibit high adsorption/photocatalytic degradation capability for RhB. In the first test, the composite aerogels exhibit the best adsorption/photocatalytic degradation performance, with 74% of the RhB removed. After the composite aerogels were separated from solution and dried, the corresponding performance decreased from 74 to 59–63% removal of RhB in subsequent recycling experiments, the performance stabilized at 63% degradation of RhB. The pores of the wet composite aerogel are initially filled with n-hexane, which has a lower surface tension than the aqueous solutions introduced during the first cycle, potentially leading to a decrease in the pore diameter and pore volume of the composite aerogel after the first cycle induced by capillary forces. As a result, the recycled composite aerogels would then be expected to have a slightly decreased adsorption/photocatalytic efficiency in the second and subsequent cycles. However, it would then be expected that the adsorption/photocatalytic efficiency of the composite aerogels for oily or gaseous pollutants would be more stable due to its nearly constant pore volume characteristic after each cycle.

4 Conclusions

Solvothermal crystallization processes controlled by BC is an effective method for synthesizing SiO_2-$W_{0.02}TiO_{2.06}$ composite aerogels with improved TiO_2 crystallization and pore volume characteristics via ambient pressure drying. The solvothermal crystallization temperature and time have a significant impact on the porosity characteristics and crystallinity of the composite aerogels. The composite aerogels with solvothermal crystallization at 120 °C for 0.5 h and 180 °C for 3 h exhibited the highest specific surface areas (416–729 m^2/g) and pore volumes (2.26–2.70 cm^3/g). With an increase of solvothermal crystallization temperature, the crystallinity of composite aerogels increased gradually. It was demonstrated that the SiO_2-$W_{0.02}TiO_{2.06}$ composite aerogels exhibited higher adsorption and degradation efficiency for RhB than the commercial P25-TiO_2, which was ascribed to the higher pore volume and specific surface area of the composite aerogels, as well as the synergistic action of adsorption and photocatalysis. Furthermore, the composite aerogel obtained with solvothermal crystallization at 180 °C for 3 h could be easily recycled many times, with the removing efficiency for RhB in the first test being 73% and stabilizing at 59–63% in the second to fourth recycling tests.

Acknowledgements This work was financially supported by the National Natural Science Foundation of China (No. 51278074, 51778098), the 2015 Liaoning Province Colleges and Universities Outstanding Talent Support Program (LR2015005), the Dalian Science and Technology Innovation Fund Project (2018J12SN066), the 2015 Science and Technology Project by the Ministry of Housing and Urban-Rural Development of China (2015-K1-042), and the 2016 Dalian City Construction Science and Technology Project (201612).

Compliance with ethical standards

Conflict of interest The authors declare that they have no conflict of interest.

Publisher's note: Springer Nature remains neutral with regard to jurisdictional claims in published maps and institutional affiliations.

References

1. Yaqubzadeh AR, Ahmadpour A, Rohani Bastami T, Hataminia MR (2016) Low-cost preparation of silica aerogel for optimized adsorptive removal of naphthalene from aqueous solution with central composite design (CCD). J Non-Cryst Solids 447:307–314

2. Meng Y, Young TM, Liu P, Contescu CI (2015) Ultralight carbon aerogel from nanocellulose as a highly selective oil absorption material. Cellulose 22:435–447
3. Bi H, Yin Z, Cao X, Xie X, Tan C, Huang X, Lu X (2013) Carbon fiber aerogel made from raw Cotton: a novel, efficient and recyclable sorbent for oils and organic solvents. Adv Mater 25:5916–5921
4. Dong S, Xia L, Guo T, Zhang F, Cui L, Su X, Wang D, Guo W, Sun J (2018) Controlled synthesis of flexible graphene aerogels macroscopic monolith as versatile agents for wastewater treatment. Appl Surf Sci 445:30–38
5. Yao X, Yu W, Xu X, Chen F, Fu Q (2015) Amphiphilic, ultralight, and multifunctional graphene/nanofibrillated cellulose aerogel achieved by cation-induced gelation and chemical reduction. Nanoscale 7:3959–3964
6. Zhou S, Jiang W, Wang T, Lu Y (2015) Highly Hydrophobic, compressible, magnetic polystyrene/Fe_3O_4/graphene aerogel composite for oil-water separation. Ind Eng Chem Res 54:5460–5467
7. Depuccio DP, Botella P, O'Rourke B, Landry CC (2015) Degradation of methylene blue using porous WO_3, SiO_2–WO_3, and their Au-loaded analogs: adsorption and photocatalytic studies. ACS Appl Mater Interfaces 7:1987–1986
8. Ahirwar D, Bano M, Khan F (2016) Synthesis of mesoporous TiO_2 and its role as a photocatalyst in degradation of indigo carmine dye. J Sol-Gel Sci Technol 79(1):228–237
9. Krumm M, Pueyo CL, Polarz S (2010) Monolithic zinc oxide aerogels from organometallic Sol−Gel precursors. Chem Mater 22:5129–5136
10. Puskelova J, Baia L, Vulpoi A, Baia M, Antoniadou M, Dracopoulos V, Stathatos E, Gabor K, Pap Z, Danciu V, Lianos P (2014) Photocatalytic hydrogen production using TiO_2–Pt aerogels. Chem Eng J 242:96–101
11. Desario PA, Pietron JJ, Devantier DE, Brintlinger TH, Stroud RM, Rolison DR (2013) Plasmonic enhancement of visible-light water splitting with Au–TiO_2 composite aerogels. Nanoscale 5:8073–8083
12. Liu JX, Shi F, Bai LN, Feng X, Wang XK, Bao L (2014) Synthesis of TiO_2–SiO_2 aerogel via ambient pressure drying: effects of sol pre-modification on the microstructure and pore characteristics. J Sol-Gel Sci Technol 69(1):93–101
13. Lázár I, Kalmár J, Peter A, Szilágyi A, Győri E, Ditrói T, Fábián I (2015) Photocatalytic performance of highly amorphous titania–silica aerogels with mesopores: The adverse effect of the in situ adsorption of some organic substrates during photodegradation. Appl Surf Sci 356:521–531
14. Heligtag FJ, Cheng W, Mendonca VRD, Suess MJ, Hamethner DG, Ribeiro C, Niederberger M (2014) Self-Assembly of metal and metal oxide nanoparticles and nanowires into a macroscopic ternary aerogel monolith with tailored photocatalytic properties. Chem Mater 26:5576–5584
15. Kovács G, Pap Z, Coteț C, Coşoveanu V, Baia L, Danciu V (2015) Photocatalytic, morphological and structural properties of the TiO_2-SiO_2-Ag porous structures based system. Materials 8:1059–1073
16. Zu G, Shen J, Wang W, Zou L, Lian Y, Zhang Z, Zhang F (2014) Robust, highly thermally stable, core–shell nanostructured metal oxide aerogels as high-temperature thermal superinsulators, adsorbents and catalysts. Chem Mater 26:5761–5772
17. Kim YN, Shao GN, Jeon SJ, Imran SM, Sarawade PB, Kim HT (2013) Sol–gel synthesis of sodium silicate and titanium oxychloride based TiO_2–SiO_2 aerogels and their photocatalytic property under UV irradiation. Chem Eng J 231:502–511
18. Setthaya N, Chindaprasirt P, Yin S, Pimraksa K (2017) TiO_2-zeolite photocatalysts made of metakaolin and rice husk ash for removal of methylene blue dye. Powder Technol 313:417–426
19. Shi F, Wang L, Liu J (2006) Synthesis and characterization of silica aerogels by a novel fast ambient pressure drying process. Mater Lett 60:3718–3722
20. Shi F, Liu JX, Song K, Wang ZY (2010) Cost-effective synthesis of silica aerogels from fly ash via ambient pressure drying. J Non-Cryst Solids 356:2241–2242
21. Shao G, Liu S, Shen X, Chen X (2017) A new rapid and economical one-step method for preparing SiO_2 aerogels using supercritical extraction. Powder Technol 312:1–10
22. Li R, Liu Y, Yan T, Li Y, Cao W, Wei Q, Du B (2015) A competitive photoelectrochemical assay for estradiol based on in situ generated CdS-enhanced TiO_2. Biosens Bioelectron 66:596–602
23. Muñoz-Batista MJ, Kubacka A, Rachwalik R, Bachiller-Baeza B, Fernández-García M (2014) Green photo-oxidation of styrene over W–Ti composite catalysts. J Catal 309:428–438
24. Sun D, Liu J, Li J, Feng Z, He L, Zhao B, Wang T, Li R, Yin S, Sato T (2014) Solvothermal synthesis of spindle-like WO_3–TiO_2 particles with enhanced photocatalytic activity. Mater Res Bull 53:163–168
25. Wang T, Tang JS, Wu S, Fan X, He J (2014) Preparation of ordered mesoporous WO_3–TiO_2 films and their performance as functional Pt supports for synergistic photo-electrocatalytic methanol oxidation. J Power Sources 248:510–516
26. Shi F, Liu JX, Huang X, Yu L, Liu SH, Feng X, Wang XK, Shao GL, Hu SC, Yang B, Fan CY (2015) Hydrothermal synthesis of mesoporous WO_3–TiO_2 powders with enhanced photocatalytic activity. Adv Powder Technol 26:1435–1441
27. Primc D, Zeng G, Leute R, Walter M, Mayrhofer L, Niederberger M (2016) Chemical substitution-alignment of the surface potentials for efficient charge transport in nanocrystalline TiO_2 photocatalysts. Chem Mater 28:4223–4230
28. Yan M, Li GL, Guo CS, Guo W, Ding DD, Zhang SH, Liu SQ (2016) WO_{3-x} sensitized TiO_2 spheres with full-spectrum-driven photocatalytic activities from UV to near infrared. Nanoscale 8:17828–17835
29. Kim HB, Kim H, Lee WI, Jang DJ (2015) Hierarchical mesoporous anatase TiO_2 nanostructures with efficient photocatalytic and photovoltaic performances. J Mater Chem A 3:9714–9721
30. Heiligtag FJ, Rossell MD, Suess MJ, Niederberger M (2011) Template-free co-assembly of preformed Au and TiO_2 nanoparticles into multicomponent 3D aerogels. J Mater Chem 211:6893–16899
31. Iguchi M, Yamanaka S, Budhiono A (2000) Bacterial cellulose—a masterpiece of nature's arts. J Mater Sci 35:261–270
32. Wang Y, Zou YC, Chen J, Li GD, Xu Y (2013) A flexible and monolithic nanocomposite aerogel of carbon nanofibers and crystalline titania: fabrication and applications. RSC Adv 3:24163–24168
33. Sai H, Xing L, Xiang J, Cui L, Jiao J, Zhao C (2014) Flexible aerogels with interpenetrating network structure of bacterial cellulose–silica composite from sodium silicate precursor via freeze drying process. RSC Adv 4:30453–30461
34. Olsson RT, Samir MA, Salazar-Alvarez G, Belova L, Ström V, Berglund LA, Gedde UW (2010) Making flexible magnetic aerogels and stiff magnetic nanopaper using cellulose nanofibrils as templates. Nat Nanotechnol 5:584–588
35. Arconada N, Castro Y, Duran (2010) A Photocatalytic properties in aqueous solution of porous TiO_2-anatase films prepared by sol-gel process. Appl Catal A 385:101–107
36. Shi F, Yu T, Hu SC, Liu JX, Yu T, Liu SH (2016) Synthesis of highly porous SiO_2–$(WO_3)_x$·TiO_2 composite aerogels using bacterial cellulose as template with solvothermal assisted crystallization. Chem Eng J 292:105–112
37. Sai HZ, Xing L, Xiang JH, Cui LJ, Jiao JB, Zhao CL, Li ZY, Li F (2013) Flexible aerogels based on an interpenetrating network of

bacterial cellulose and silica by a non-supercritical drying process. J Mater Chem A 1:7963–7970
38. Liu D, Shi F, Liu J, Hu S, Yu L, Liu S, Wang Y, Shan Z, Liu J, Tian X (2017) Synthesis of SiO_2-W_xTiO_2 composite aerogels via solvothermal crystallization under the guidance of bacterial cellulose followed by freeze drying method. J Sol-Gel Sci Technol 84:42–50
39. Wang X, Liu J, Shi F, Liu S, Feng X, Bao L (2014) Influences of heat-treatment on the microstructure and properties of silica-titania composite aerogels. J Porous Mater 21:293–301
40. Wang F, Zhang S, Li C, Liu J, He S, Zhao Y, Duan X (2014) Catalytic behavior of supported Ru nanoparticles on the (101) and (001) facets of anatase TiO_2. RSC Adv 4:10834–10840
41. Kanamori K, Aizawa M, Nakanishi K, Hanada T (2007) New transparent methylsilsesquioxane aerogels and xerogels with improved mechanical properties. Adv Mater 19:1589–1593
42. Yun S, Luo H, Gao Y (2014) Ambient-pressure drying synthesis of large resorcinol–formaldehyde-reinforced silica aerogels with enhanced mechanical strength and superhydrophobicity. J Mater Chem A 2:14542–14549
43. Huang X, Liu JX, Shi F, Yu L, Liu SH (2016) Ambient pressure drying synthesis of $Cs_{0.33}WO_3/SiO_2$ composite aerogels for efficient removal of Rhodamine B from water. Mater Des 110:624–632
44. Iturbe-Ek J, Andrade-Martinez J, Gomez R, Rodriguez-Gonzalez V (2015) A functional assembly of SiO_2 nanospheres/Graphene oxide composites. Mater Lett 142:75–79
45. Yan X, Ohno T, Nishijima K, Abe R, Ohtani B (2006) Is methylene blue an appropriate substrate for a photocatalytic activity test? A study with visible-light responsive titania. Chem Phys Lett 429:606–610